# Uniformity detector retinal ganglion cells fire complex spikes and receive only light-evoked inhibition

Benjamin Sivyer[a], W. Rowland Taylor[b], and David I. Vaney[a,1]

[a]Australian Research Council Centre of Excellence in Vision Science, Queensland Brain Institute, University of Queensland, Brisbane 4072, Queensland, Australia; and [b]Casey Eye Institute, Oregon Health and Science University, Portland, OR 97239

Edited* by John E. Dowling, Harvard University, Cambridge, MA, and approved January 28, 2010 (received for review August 24, 2009)

**Retinal ganglion cells convey information by increasing their firing in response to an optimal visual stimulus or "trigger feature." However, one class of ganglion cell responds to changes in the visual scene by decreasing its firing. These cells, termed uniformity detectors in the rabbit retina, are encountered only rarely and the synaptic mechanisms underlying their unusual responses have not been investigated. In this study, patch-clamp recordings of uniformity detectors show that the action potentials underlying the maintained firing arise within "complex spikes." Both ON and OFF visual stimuli elicit only inhibitory synaptic input, the immediate effect of which is to suppress the maintained firing. However, this inhibition also alters the properties of the "renascent" spiking by increasing the amplitude of the spikes within each burst, suggesting that the effect may increase the efficacy of spike propagation and transmission.**

calcium spike | glycine | Na-channel inactivation | rabbit | suppressed by contrast

Uniformity detector (UD) retinal ganglion cells (RGCs) were first described in the rabbit by Levick (1) and appear to be homologous to the suppressed-by-contrast RGCs described in the cat (2) and the primate (3).

There are approximately a dozen other classes of RGCs in the rabbit, all of which increase their firing in response to appropriate visual stimuli (4–7). By contrast, the UDs fire continuously under steady illumination but are suppressed by lighter (ON) or darker (OFF) stimuli projected on the receptive field. These cells reportedly comprise two types: One type shows transient suppression to visual contrast, whereas the other type shows sustained suppression (1, 8–11).

Amthor et al. (8) recorded from a sustained UD in the rabbit retina and filled it with dye. The RGC had a distinctive bistratified morphology, branching at both the inner and outer margins of the inner plexiform layer, in the ON- and OFF-sublaminae, respectively. Golgi-stained RGCs with a matching morphology were characterized by Famiglietti (12), who called them type 2 bistratified (BS2) cells to distinguish them from the commonly encountered ON-OFF direction-selective RGCs (BS1 cells). The BS2 cells have comparatively large dendritic fields and Famiglietti estimated that <1% of RGCs would be required for efficient tiling of the presumptive UDs across the retina.

Such scarcity, together with the peculiar receptive-field properties, would explain why UDs were encountered infrequently in early physiological surveys of rabbit RGCs; indeed, more recent population studies on the rabbit retina have not reported finding any UDs (13) or BS2 RGCs (14). Consequently, our understanding of UDs has progressed little in the 40 years since they were discovered by Levick (1), and the mechanisms underlying their curious responses have not been investigated.

In this study, we have been able to microscopically target UDs with a high success rate in a whole-mount preparation of the rabbit retina, thereby allowing patch-clamp recordings to be made from a large sample of these cells. We made a detailed examination of the synaptic inputs that underlie the receptive-field properties of the UDs, and also characterized the intrinsic mechanisms that generate their maintained firing.

Interestingly, the UDs produce complex spikes, unlike other classes of RGCs. First described by Eccles and colleagues (15), complex spikes are bursts of $Na^+$ spikelets that ride on top of a slower $Ca^{2+}$-mediated depolarization (16). They are known to serve diverse functions in a variety of neuronal populations elsewhere in the CNS (17–20). Here, we show how light-evoked inhibition has various effects on the properties of complex spikes in UDs.

## Results

**Physiological and Morphological Identification.** Electrophysiological recordings of RGCs were made in a dark-adapted whole-mount preparation of the rabbit retina, which was placed photoreceptor-side down in a brain-slice chamber on a fixed-stage microscope (21, 22). The RGC somata were visualized under infrared illumination, and an extracellular electrode was applied to the targeted soma under microscopic control. Spike recordings were made in the loose-patch configuration, and the RGCs were rapidly screened by mapping their responses to a light or dark spot flashed over the receptive field. Although most RGCs fired at light ON or light OFF, a small proportion had receptive-field properties that resembled those of UDs described in previous studies on the rabbit retina. It became clear that these cells had a medium-sized round soma whose nucleus was not distinct and, when this gestalt was used to target the cells, the UDs could be encountered with high reliability.

Under steady illumination, the UDs showed a maintained firing rate of ≈20 spikes/s, which was transiently eliminated at the onset and termination of either a light or dark spot flashed over the receptive field (Fig. 1*A*). All tested visual stimuli transiently suppressed the maintained firing, including bars or gratings moved in any direction through the receptive field, although whole-field stimuli produced less suppression than localized stimuli. We can exclude the possibility that these properties reflected systemic problems with the preparation because other classes of RGCs recorded before or after the UDs fired robustly when stimulated with flashing spots and moving stimuli. Recordings from 13 UDs under photopic illumination showed that the response suppression to a flashing black spot was fairly consistent across the population (Fig. 1 *B* and *C*). The maintained firing was totally suppressed for 0.5–1 s at light OFF and then largely recovered over the next 3–5 s; the suppression at light ON showed a similar time course. UDs displayed qualitatively similar response properties regardless of whether they were stimulated under scotopic, mesopic, or photopic conditions with green light (518 nm peak), or with blue light (445 nm peak) that would selectively activate the short-wavelength cones.

After extracellular recordings, many UDs were filled with Neurobiotin by using a loose-patch electroporation technique (23) and they all showed a distinctive bistratified morphology. The UDs

Author contributions: B.S. and W.R.T. designed research; B.S. performed research; B.S. and W.R.T. analyzed data; and B.S., W.R.T., and D.I.V. wrote the paper.

The authors declare no conflict of interest.

*This Direct Submission article had a prearranged editor.

[1]To whom correspondence should be addressed. E-mail: d.vaney@uq.edu.au.

This article contains supporting information online at www.pnas.org/cgi/content/full/0909621107/DCSupplemental.

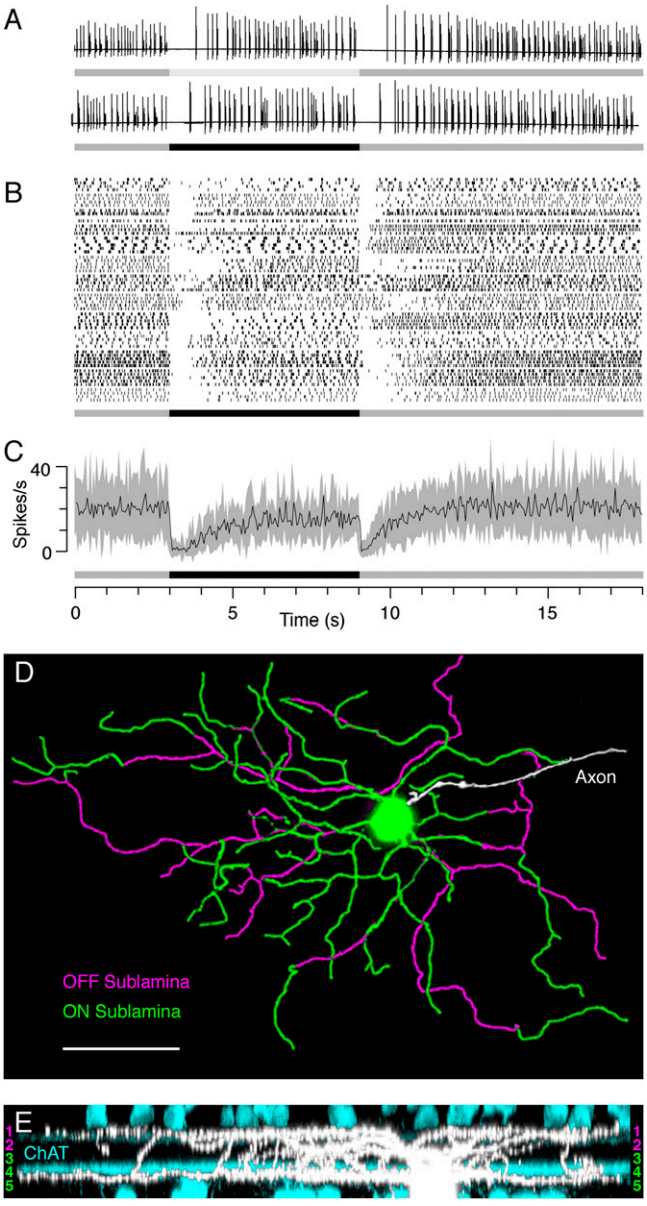


**Fig. 1.** Uniformity detectors (UDs) show maintained firing that is suppressed at light ON and light OFF and they have bistratified dendritic trees. (*A*) Extracellular recording of the spike responses of a UD to a light spot (*Upper*) and a dark spot (*Lower*) flashed in the receptive field; the light and dark bars show the 6-s duration of the flash. (*B*) Spike raster plots from 13 UDs in response to 3–5 trials of a flashing dark spot. (*C*) Average spike rate (± SD, gray shading) for the 13 raster plots. (*D*) Tracing of the dendritic morphology of a Neurobiotin-filled UD reconstructed from a confocal *z* series. (Scale bar: 50 μm.) Characteristically, some of the dendrites in the proximal ON sublamina of the inner plexiform layer (green) arise retroflexively from dendrites in the distal OFF sublamina (magenta). (*E*) Vertical projection of the same cell (white) showing the dendritic stratification in relation to strata 1–5 of the inner plexiform layer and the populations of starburst amacrine cells, labeled with an antibody against choline actyltransferase (ChAT, blue).

located ≈0.5 mm inferior of the visual streak had a relatively large dendritic tree with an equivalent diameter of ≈250 μm. The sparsely branched dendrites of the UDs, which often followed a meandering course, branched largely within two strata near the margins of the inner plexiform layer, one in the ON sublamina and the other in the OFF sublamina (Fig. 1*D*). In tissue immunolabeled for choline acetyltransferase, the actual levels of stratification could be gauged relative to those of the OFF and ON starburst amacrine cells, which stratify at ≈22% and 69% depth of the inner plexiform layer, respectively. The proximal dendrites of the UDs were located just below the ON starburst cells, whereas the distal dendrites were mostly located above the OFF starburst cells (Fig. 1*E*). Interestingly, all of the Neurobiotin-injected UDs had dendrites that dived retroflexively from the OFF sublamina to the ON sublamina, so that the ON dendrites arose not only from the adjacent soma but also indirectly from the OFF dendrites.

**Visual Stimuli Elicit Only Inhibition.** Like other neurons, the output of RGCs is determined in large measure by the balance between excitatory and inhibitory inputs and their temporal interactions (7, 21, 22). Although visual stimuli clearly suppress the maintained firing of UDs, no recordings of the cells' intracellular responses have been published, and it is not known whether the spike suppression arises from decreased excitatory input from bipolar cells, increased inhibitory input from amacrine cells, or a combination of the two.

We addressed this issue by making patch recordings from UDs in voltage-clamp mode. When the cells were clamped at the $Cl^-$ reversal potential, the light-evoked currents were almost totally suppressed and, moreover, the currents reversed either side of the reversal potential, indicating that the light-evoked input to the UDs is largely inhibitory (Fig. 2*A*). We then extended this analysis quantitatively by voltage-clamping UDs at a range of holding potentials from –100 mV to +10 mV while presenting the same visual stimulus. The light-evoked synaptic conductance was calculated, as described by Borg-Graham (24) and Taylor and Vaney (21), and the excitatory ($G_e$) and inhibitory ($G_i$) components were plotted, based on the calculated reversal potentials of 0 mV for cation channels and –73 mV for $Cl^-$ channels.

In response to a flashed dark spot (Fig. 2*B*), UDs showed a large inhibitory conductance at both the stimulus onset (OFF response: integrated $G_i$ = 4.8 ± 4.0 nS.s; $n$ = 23) and termination (ON response: integrated $G_i$ = 6.7 ± 4.6 nS.s). Surprisingly, excitatory conductance was essentially absent at both the stimulus onset

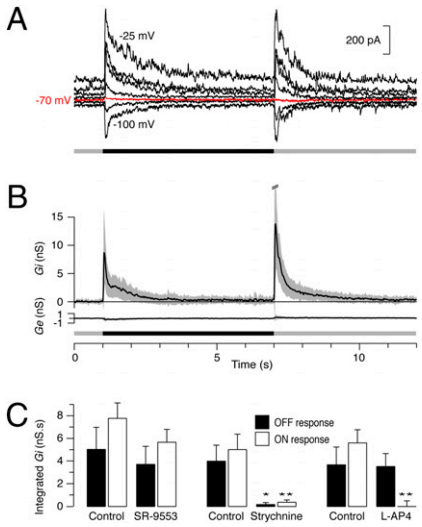


**Fig. 2.** Visual stimuli evoke transient inhibitory inputs that are mediated by glycinergic amacrine cells. (*A*) Voltage-clamp recording from a UD that was held at a range potentials from –100 mV to –25 mV while a dark spot was flashed in the receptive field. When the cell was clamped at –70 mV (red trace), close to the calculated inhibitory reversal potential of –73 mV, the large synaptic currents transiently evoked at light OFF and light ON disappeared. (*B*) Calculated mean (± SD) synaptic inhibitory conductance ($G_i$) and excitatory conductance ($G_e$) evoked by a flashing dark spot in 23 UDs. (*C*) The integrated inhibitory conductance (± SEM) of the OFF response (filled bars) and ON response (open bars) to a flashing dark spot while the retina was superperfused with 10 μM SR-95531 ($n$ = 5), 1 μM strychnine ($n$ = 7; $P$ = 0.019 OFF, $P$ = 0.005 ON), and 20 μM L-AP4 ($n$ = 4; $P$ = 0.5 OFF, $P$ = 0.001 ON).

(OFF response: integrated $G_e = -0.2 \pm 0.6$ nS.s) and termination (ON response: integrated $G_e = 0.4 \pm 0.6$ nS.s), indicating that the transient suppression of firing of UDs is mediated by the activation of transient inhibition and not by the removal of tonic excitation. The inhibitory conductance was fast rising, peaked quickly and decayed quite rapidly: For both the mean ON and OFF responses, $G_i$ had dropped to ≈15% of the peak values within 1 s of the stimulus onset, corresponding to the period of spike suppression.

The calculated inhibitory conductance ($G_i$) reflects the change in inhibitory conductance induced by the visual stimulus, with the average $G_i$ prior to stimulation set to 0. The voltage-clamp recordings showed that the UDs received a low frequency of irregular spontaneous currents that reversed close to the inhibitory reversal potential (Fig. S1*A*), indicating that they comprised only inhibitory postsynaptic currents (IPSCs) and not excitatory postsynaptic currents (EPSCs). The waveform of the averaged IPSCs at each holding potential (Fig. S1*B*) was calculated for five UDs and a regression line fitted to the current/voltage (IV) relations for the grouped data (Fig. S1*C*). The average IPSC had a conductance of $830 \pm 50$ pS and the reversal of the fitted line was –71.5 mV, close to the calculated reversal potential for inhibitory currents (–73 mV).

**Inhibitory Input Is Glycinergic.** Approximately half the amacrine cells in the retina use the inhibitory transmitter GABA and the other half use the inhibitory transmitter glycine (25). We examined the effects of bath application of the $GABA_A$-receptor blocker, 10 μM SR-95531, and the glycinergic antagonist, 1 μM strychnine, on the synaptic inputs to UDs (Fig. 2*C*). SR-95531 caused a small decrease in the integrated inhibitory conductance, but the effect was not significant for either the ON response ($P = 0.2, n = 5$) or the OFF response ($P = 0.7$). By contrast, strychnine reduced the stimulus-evoked inhibitory conductance by 92% for the ON response ($P = 0.005, n = 7$) and 95% for the OFF response ($P = 0.02$). Moreover, the isolated IPSCs apparent prior to stimulation were also abolished by strychnine. These results indicate that the light-evoked inhibitory inputs to UDs are mediated overwhelmingly by glycinergic amacrine cells. The small residual inhibition that remained in the presence of strychnine appears to be mediated by GABAergic receptors. Neither the glycinergic nor GABAergic antagonists, alone or in combination, unmasked a direct light-evoked excitatory input to the UDs.

To differentiate the roles of the ON and OFF bipolar cells in the UD circuitry, the photoreceptor input to the ON bipolar cells was blocked with bath application of the mGluR6 agonist, L-AP4 (20 μM). The effects on the UDs were clear-cut (Fig. 2*C*): The ON inhibitory input was completely abolished ($P = 0.002, n = 4$), whereas the OFF inhibitory input was not significantly affected ($P = 0.5$). Taken together with the effects of the inhibitory antagonists, these results suggest that the neuronal circuitry underlying the response properties of UDs is duplicated in the ON and OFF sublaminae, reflecting the cell's bistratification. However, we cannot discount the possibility that a single type of ON-OFF glycinergic amacrine cell provides the inhibitory inputs to both the ON and OFF stratifications.

Whole-field stimuli produced less suppression of spiking than localized stimuli and, correspondingly, conductance analysis showed that whole-field stimuli elicited less inhibitory input. These findings indicate that the glycinergic amacrine cell is itself inhibited by wide-field amacrine cells, which are probably GABAergic (25). Such wide-field inhibition could act either directly on the glycinergic amacrine cell or indirectly on the bipolar cells that are presynaptic to the amacrine cell.

**UDs Generate Complex Spikes.** The extracellular recordings revealed that the UDs fired bursts of action potentials both under steady illumination and during periods of changing visual stimulation. These bursts are unusual as the spikes within each burst were quite variable in amplitude, with the first spike usually being the largest. The bursts were highly regular ($8.1 \pm 0.9$ bursts/s, $n = 11$) and typically contained 2–3 spikes per burst. This striking pattern was such a characteristic feature of the UDs that the cells could be reliably identified from their maintained firing alone, before the cell was tested with any visual stimuli. Although previous studies have not commented on the burst firing of UDs, it is apparent in some of the published spike records (9, 26).

Perforated-patch recordings under current clamp revealed that the bursts of action potentials ride on rhythmic depolarizing waves of ≈50–100 ms duration and ≈10 mV amplitude (Fig. 3*A*). Within each burst, the larger first spike was triggered by the relatively fast-rising wavefront, whereas the smaller spikes (spikelets) rode on the wave top. The spikes but not the slow depolarizations were reversibly abolished by 100 nM tetrodotoxin (TTX), whereas the slow depolarisations, but not the spikes, were eliminated by 500 μM $Cd^{2+}$, a calcium channel blocker, indicating they are mediated by a $Ca^{2+}$-dependent mechanism. Such brief bursts of voltage-gated $Na^+$ action potentials driven by a slow $Ca^{2+}$-mediated depolarization are termed "complex spikes" (16, 27); they are found throughout the CNS but have not been previously reported in the retina.

**Modulation of Burst Frequency.** The slow depolarizations of complex spikes are usually driven by either extrinsic synaptic inputs or intrinsic $Ca^{2+}$-dependent mechanisms (16, 28, 29) although, in some neurons, rhythmic bursting is generated by persistent $Na^+$ currents (30). The burst firing of UDs persisted during bath application of a cocktail of synaptic blockers (CNQX, L-AP4, D-AP5, picrotoxin, strychnine, hexamethonium), suggesting that the bursting is generated intrinsically. However, the synaptic blockers decreased the burst frequency from $7.8 \pm 0.5$ SEM to $0.97 \pm 0.04$

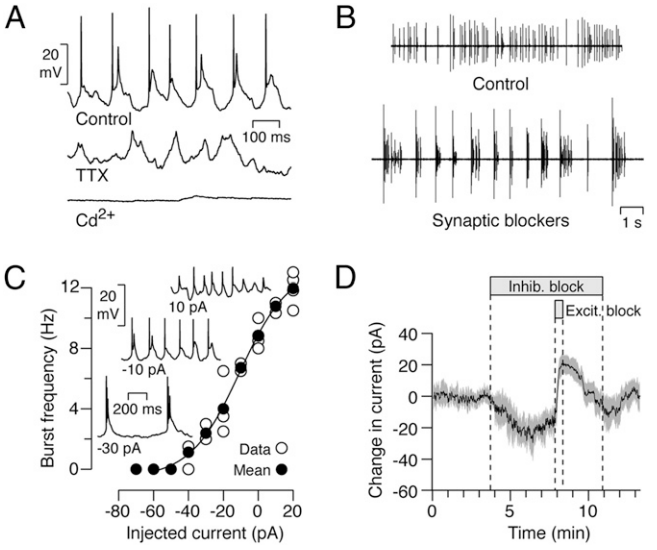


**Fig. 3.** UDs produce complex spikes whose burst frequency is modulated by hyperpolarization. (*A*) The complex spikes of UDs comprise fast spikes riding on a slow depolarization (Control); the spikes are abolished by 100 nM tetrodotoxin (TTX), whereas the slow depolarizations are abolished by a calcium-channel blocker (500 μM $Cd^{2+}$). (*B*) A cocktail of synaptic blockers reduces the burst frequency of UDs. (*C*) Polarization of UDs by current injection modulates the burst frequency and spike amplitude of complex spikes. The mean burst frequency (filled circles) of 4 cells (open circles) is plotted against the injected current in current-clamp mode; *Insets* show sample voltage traces for 10, –10, and –30 pA current injection. (*D*) The application of inhibitory blockers produces a net inward current in voltage-clamp mode; coapplication of excitatory blockers results in a transient outward shift in the measured current that exceeds the baseline current, indicating that UDs receive a tonic excitatory input (mean current ± SEM, $n = 5$).

SEM bursts/s ($n$ = 6; Fig. 3*B*), indicating that the frequency of bursting is modulated extrinsically.

In current-clamp mode, hyperpolarization of the UD by negative current injection reduced the burst frequency ($n$ = 4; Fig. 3*C*). This finding raises the possibility that the cocktail of synaptic blockers may reduce the burst frequency by suppressing tonic depolarizing excitatory input (31). To test whether UDs receive tonic synaptic inputs, we clamped the cells at –70 mV and applied a cocktail of inhibitory blockers (strychnine, SR-95531, TPMPA, CGP-35348), followed by a combination of the inhibitory blockers plus excitatory blockers (CNQX, L-AP4, D-AP5, hexamethonium). The wash-in of the inhibitory blockers produced a negative (inward) shift in the current (–26 ± 4 SEM pA), consistent with the removal of a tonic (outward) inhibitory input (Fig. 3*D*). This result was not unexpected because we had shown that spontaneous IPSCs are present in the absence of visual stimulation.

The wash-in of the excitatory blockers on top of the inhibitory blockers produced a positive (outward) shift in the current (45 ± 6 SEM pA), consistent with the removal of a tonic (inward) excitatory input. Moreover, the fact that the combined blockers produced a net positive shift relative to control conditions (19 ± 3 SEM pA) indicates that UDs normally receive a tonic excitatory input. However, the blocking experiments do not tell us about the relative weights of the tonic excitatory and inhibitory inputs under normal conditions. Similar results were obtained by including only one excitatory blocker, CNQX, suggesting that the tonic excitatory input is AMPA-kainate mediated.

**Light-Evoked Inhibitory Modulation of Spike Amplitudes.** Perforated-patch recordings under current clamp ($n$ = 4) showed that the strong inhibitory inputs at light OFF and light ON transiently hyperpolarized the UDs by ≈20 mV, from a baseline potential of –50.2 ± 1.6 mV to –71.6 ± 1.0 mV, close to the predicted $Cl^-$ reversal potential (Fig. 4*A*). The cells returned to near the resting potential over a period of ≈5 s, with complex spikes reappearing when the baseline potential approached –60 mV, ≈1 s after the stimulus onset or termination. The complex spikes that arise after the transient spike suppression, while the cell is still hyperpolarized, are here termed "renascent" spikes.

The complex spikes produced during maintained firing and renascent firing were qualitatively similar in that the absolute peak voltage of the first spike was always greater than that of the following spikes. It was apparent, however, that the renascent spikes were larger, the interspike interval was shorter, and a third spike was commonly generated (Fig. 4*B*). Quantitative analysis of the current-clamp recordings ($n$ = 4) showed how the absolute peak voltage and the maximal rate of rise (dV/dt) of the first and second spikes of a burst varied with the light-evoked hyperpolarization. In the initial renascent bursts, the absolute peak voltage of the first spike increased by ≈11 mV and the second spike almost doubled in amplitude, reaching an absolute peak voltage of approximately –8 mV, comparable with that of the first spike prior to stimulation (Fig. 4*C*). These light-evoked changes in spike amplitude were also apparent in extracellular recordings (Fig. S2) and were mimicked by negative current injection.

The larger amplitude of the renascent spikes, resulting from both the more positive peak voltage and the more negative spike threshold, was also reflected in the rate of voltage rise (dV/dt; Fig. 4*D*). In the initial renascent bursts, the maximal rate of rise almost doubled for the first spike and was approximately five times greater for the second spike (Fig. 4*D*).

Such larger, faster spikes are consistent with a higher effective Na channel density, which could occur if the light-evoked hyperpolarization removed inactivation of voltage-gated $Na^+$ channels. To test this hypothesis, we plotted the amplitudes of the first and second spikes measured under current clamp against the spike threshold (Fig. 4*E*) and compared the threshold range to the voltage dependency of $Na^+$-channel inactivation measured under voltage clamp (Fig. S3) in five other UDs (Fig. 4*F*). These data indicate that spikes

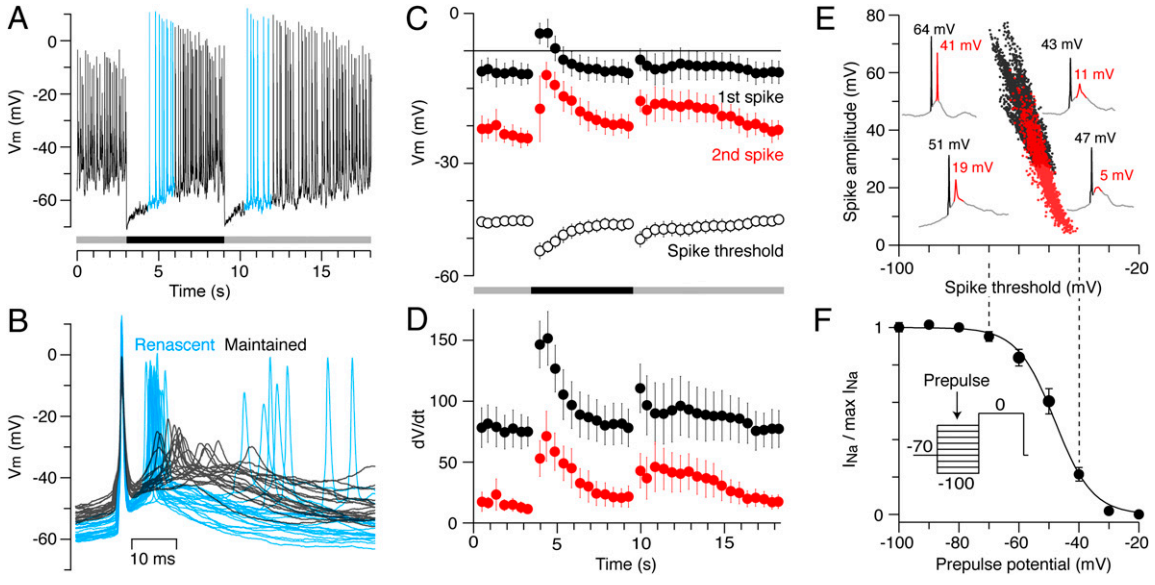


**Fig. 4.** Light-evoked hyperpolarization of the UDs increases the amplitude of the renascent spikes, reflecting removal of voltage-gated $Na^+$-channel inactivation. (*A*) Perforated-patch current-clamp recording from a UD in response to a flashed dark spot. (*B*) Complex spikes aligned to the peak voltage of the first spike; renascent spikes (blue) are larger, faster, and more likely to produce a third spike than maintained spikes (black). (*C–E*) The effects of light-evoked hyperpolarization on the properties of complex spikes ($n$ = 4, ± SEM.). (*C*) The absolute peak voltage of the first spike (black circles) and second spike (red circles) within each burst, and the spike threshold of the first spike (open circles); the spike threshold was measured 1 ms prior to the rate of rise reaching 40 V/s and reflected the initial membrane potential. (*D*) The maximum rate of rise (dV/dt) of the first spike (black circles) and second spike (red circles). (*E*) Individual spike amplitudes for the first spike (black symbols) and second spike (red symbols) plotted against the spike threshold; example traces are taken from the cell in *A*, illustrating the variability in amplitudes of the first (black) and second (red) spikes. (*F*) Mean steady-state inactivation ($n$ = 5, ± SEM) of $Na^+$ currents measured by prepulses at different potentials (*Inset*) and fitted with a Boltzmann function (solid line; $V_{half}$ = –48 mV, $k$ = 6.3 mV); the onset of inactivation mirrors the decline in spike amplitude and increase in spike thresholds mapped in *E*. Pulse protocol: holding potential at –70 mV, 50 ms prepulse at potentials from –100 mV to –20 mV in 10-mV steps, and 100-ms test pulse at 0 mV.

with the largest amplitudes activate at voltages where almost all $Na^+$ channels are available whereas, at the threshold voltages for the smallest spikes, only ≈30% of the $Na^+$ channels are available.

## Discussion

Here we have shown that the rabbit retina contains a homogeneous population of UD RGCs whose morphological and physiological properties were consistent across a large sample of cells. The UDs, which had a distinctive bistratified morphology, fired bursts of complex spikes that were transiently suppressed at light ON and light OFF. This suppression was driven by transient light-evoked glycinergic inhibition, with the UDs appearing to receive negligible light-evoked excitatory input. In this regard, they are unlike other classes of RGC, including the intrinsically photosensitive RGCs, all of which are depolarized by light-evoked glutamatergic input from bipolar cells (13, 32, 33). Although the UDs do appear to receive a small tonic excitatory input, which may set the frequency of the maintained bursts, the puzzle remains as to why this input does not appear to be modulated by visual stimuli known to activate bipolar cells.

The homogeneity of the UDs was somewhat unexpected, given earlier reports that UDs comprise both transient- and sustained-response types. We targeted somata with a particular gestalt and did not conduct a systematic survey of all the RGCs. However, extracellular recordings were made from many other types of RGCs during the course of this study, but none appeared to be sustained UDs. By contrast, Levick (1) only illustrated sustained cells in his original description of UDs—also recorded on the rabbit visual streak—and simply noted that "others were only transiently (~0.5 sec) stopped by the stimuli". Interestingly, the sustained UD recovered by Amthor et al. (8) showed a similar branching pattern and bistratification to our transient UDs, which possibly correspond morphologically to the BS2 RGCs of Famiglietti (12). It seems possible that there may not be distinct transient and sustained types of UDs but, rather, their physiological responses may depend on factors such as adaptational state or level of anesthesia.

The current-clamp recordings showed that UDs produced rhythmic bursts of complex spikes that were driven by slow depolarizations, probably arising from an intrinsic $Ca^{2+}$-dependent mechanism. The name "uniformity detector" or "suppressed-by-contrast cell" implies that the initial suppression of spiking is the salient signal conveyed to the higher visual centers and, indeed, this was the most obvious feature of the extracellular spike records. However, it is possible that the renascent spiking also conveys important information, notwithstanding the long delay between the onset of the visual stimulus and the renascent spiking (0.5–1 s for flashing spots). The visual-evoked hyperpolarization produced significant increases in the amplitude and maximal rate of rise (dV/dt) of both the first and second spikes recorded at the soma. This effect was particularly pronounced for the initial renascent second spikes, whose properties approached those of the maintained first spikes.

Unlike simple spikes, which are transmitted with high fidelity, the $Na^+$ spikes of complex spikes often fail to propagate down the axon (34, 35) or to induce a postsynaptic response (19, 36). In both Purkinje cells and cartwheel cells, spikelet propagation and transmission success are closely correlated with the peak voltage of the spikelet and the maximal rate of rise. In cartwheel cells, most transmission failures correspond to spikelets that are small, slow to rise, and preceded by depolarized membrane potentials (19). Correspondingly in Purkinje cells, hyperpolarization increases the transmission of spikelets that fail to propagate at more depolarized potentials (35).

It therefore seems possible that the second spikes of the UDs are only propagated for the hyperpolarized renascent bursts, although we have no recordings from the unmyelinated portion of the axon within the retina, or the myelinated portion in the optic nerve or optic tract, to test this hypothesis. The consequences of such thresholding could be pronounced. The rate of firing of the renascent spikes in the axon would actually be greater than the maintained firing rate, contrasting with the accepted wisdom that visual stimulation does not increase the firing rate of UDs; moreover, the close apposition (≈10 ms) of the spike pair in each burst might greatly facilitate neurotransmitter release (37). In fact, spike recordings of suppressed-by-contrast cells in the cat retina show "postsuppression facilitation," where the renascent firing is greater than the maintained firing (10, 38). Moreover, the raster plots and spike-time histogram of the UD spiking would also have exhibited postsuppression facilitation if an intermediate spike-detection level had been selected.

The inhibitory inputs activated by visual stimuli have two contrasting effects on the UDs. Stronger inhibition that reduces the membrane potential below approximately –60 mV suppresses the spiking of the cells, whereas weaker inhibition that hyperpolarizes the cell by a smaller amount boosts the complex spikes of the cells. Although these two effects are temporally distinct for artificial visual stimuli like the high-contrast flashing spots used in this study, the challenge for the future will be to understand how UDs respond to low-contrast natural scenes when filtered through the prism of the animal's head and eye movements.

## Materials and Methods

**Retina Preparation and Visual Stimulation.** Experiments were conducted in accord with the Australian Code of Practice, and the protocols were approved by the Animal Ethics Committee at the University of Queensland. Dark-adapted adult pigmented rabbits of either sex were anesthetized (12 mg/kg ketamine, 12 mg/kg i.m.) before being overdosed with pentobarbitone sodium (150 mg/kg i.v.). The eyes were then quickly enucleated, hemisected, and placed in carbogenated Ames solution at room temperature (pH 7.4). The retina was dissected from the sclera under infrared (IR) illumination, placed in a recording chamber (Warner, 26-GLP), held by a slice anchor (Warner, SHD 26GH/2), and perfused at 5 mL/min with Ames medium at 34 °C. The recording chamber was placed on a fixed-stage Olympus BX-51 microscope with a dual-magnification port, which allowed simultaneous light stimulation of the retina at ×20 (≈1 mm diameter) and visualization of the RGC somata at ×80 by using IR gradient-contrast optics (39). Visual stimuli were generated by using custom software (Igor Pro) and presented on a 800 × 600 pixel green-phosphor OLED screen (Emagin OLED-XL microdisplay; 518-nm peak). In most experiments, the background illumination was maintained above the level of rod saturation at ≈3.5 $e^{11}$ quanta/$cm^2$ per sec and the visual stimuli were set at ±50% of the background (1.75 $e^{11}$ quanta/$cm^2$ per sec for OFF stimuli; 5.25 $e^{11}$ quanta/$cm^2$ per sec for ON stimuli). A flashing light spot of 300 μm diameter was centered over the RGC soma and focused on the photoreceptor outer segments. Moving bars (200 × 300 μm, 200 μm/s), moving square-wave gratings (full field, 200 μm spatial period) and a range of spot sizes (50–1,200 μm) were also used to test the receptive-field properties in different cells.

**Electrophysiology and Data Analysis.** Recordings were made on a HEKA EPC-10 patch-clamp amplifier with electrodes pulled from borosilicate glass to a resistance of 3–5 MΩ. Extracellular electrodes were filled with Ames solution and patch electrodes for voltage-clamp recordings were filled with an intracellular solution containing: 125 mM Cs-methanesulphonate, 5 mM Na-HEPES, 1 mM EGTA, 3 mM Mg-ATP, 300 μM Tris-GTP, 10 mM phosphocreatine, 5 mM TEA-Cl, 3 mM lidocaine N-ethyl chloride (QX-314), balanced to pH 7.2 with cesium hydroxide. QX-314 was included in the patch electrode to block action potentials and nonlinear voltage-gated currents, for the $Na^+$-inactivation experiments, QX-314 was excluded and the $Cl^-$ concentration was balanced with 3 mM NaCl. For the perforated-patch current-clamp recordings, QX-314, phosphocreatine, ATP, and GTP were excluded, 240 μg/mL amphotericin-B and 3 mM KCl were included, and the $Cs^+$ was replaced by $K^+$ (40). The measured liquid junction potential, 10 mV for the Cs solutions and 9 mV for the $K^+$ solution, was subtracted from all traces, and the series resistance was routinely compensated online. The series resistance averaged 15 ± 4 MΩ ($n$ = 14), and UDs had an average input resistance, capacitance, and mean membrane potential of 192 ± 21 MΩ ($n$ = 14), 12 ± 2 pF ($n$ = 14), and –51 ± 2 mV ($n$ = 4), respectively. The mean membrane potential was calculated offline after removing the fast component of the maintained action potentials from the current-clamp recordings. The following concentrations of reagents were used to test the pharmacology of synaptic inputs: CNQX 100 μM (Tocris), D-AP5 100 μM (Tocris), L-AP4 20 μM (Tocris), hexamethonium 100 μM (Sigma), picrotoxin 100 μM (Sigma), strychnine 1 μM (Sigma), SR-95531 10 μM (Sigma), TPMPA 50 μM (Tocris), and CGP-35348 100 μM (Tocris). The calculation of the excitatory and inhibitory components of the light-evoked synaptic inputs has been described in detail (21, 24). Briefly, the visual stimulus was repeated while voltage clamping the RGCs at a range of potentials (–100 to +10 mV in 10- to 15-mV increments). IV relations of the net light-evoked current were generated at 10-ms time intervals for the duration of the light stimulation. The linear

regression fit to each IV was accounted for by a sum of linear excitatory and inhibitory conductance components with reversal potentials of 0 and –73 mV, respectively. Errors are standard deviations unless otherwise noted. For spike analysis, the first spike in a burst was defined as having a peak dV/dT > 40 V/s and not preceded by another spike by less than 50 ms. The second spike in the burst was defined as an event with a maximal dV/dT > 5 V/s; subsequent spikes, if present, were ignored. In each cell, the accuracy of the automated analysis algorithm was verified by manually inspecting a fraction of the identified spikes. These criterion values for identifying spikes were arrived at empirically, and the outcome of the analysis was not critically dependent on these precise values.

**Dendritic Morphology.** RGCs were filled with Neurobiotin by using a semiloose seal electroporation technique, as described by Kanjhan and Vaney (23). After fixation for 30 min in 4% paraformaldehyde in 0.1 M PBS and overnight washing in PBS, the retina was incubated in blocking solution (PBS containing 1% IgG-free BSA (Jackson ImmunoResearch), 1% normal donkey serum (Jackson ImmunoResearch), 0.5% Triton X-100, 0.2% sodium azide) with goat anti-choline acetyltransferase (1:1000; Chemicon; AB144P) for 5 days at room temperature. The retina was washed overnight and then incubated overnight at room temperature in blocking solution containing Cy-3 streptavidin (1:500; Jackson ImmunoResearch) and Cy-5 donkey anti-goat (1:500; Jackson ImmunoResearch). The dendritic morphology and stratification of the RGCs were reconstructed by confocal microscopy (Zeiss; LSM-510 meta).

**ACKNOWLEDGMENTS.** We thank Nick Nacsa for technical assistance and Rowan Tweedale and Angelique Paulk for critically reading the manuscript. This work was supported by Australian Research Council Centre of Excellence Grant CE0561903 (to D.I.V.), National Health and Medical Research Council of Australia grants (to D.I.V.), National Eye Institute Grant EY014888 (to W.R.T.), and a University of Queensland scholarship (to B.S.).

1. Levick WR (1967) Receptive fields and trigger features of ganglion cells in the visual streak of the rabbits retina. *J Physiol* 188:285–307.
2. Rodieck RW (1967) Receptive fields in the cat retina: A new type. *Science* 157:90–92.
3. de Monasterio FM (1978) Properties of ganglion cells with atypical receptive-field organization in retina of macaques. *J Neurophysiol* 41:1435–1449.
4. Caldwell JH, Daw NW (1978) New properties of rabbit retinal ganglion cells. *J Physiol* 276:257–276.
5. Devries SH, Baylor DA (1997) Mosaic arrangement of ganglion cell receptive fields in rabbit retina. *J Neurophysiol* 78:2048–2060.
6. Vaney DI, Levick WR, Thibos LN (1981) Rabbit retinal ganglion cells. Receptive field classification and axonal conduction properties. *Exp Brain Res* 44:27–33.
7. Roska B, Molnar A, Werblin FS (2006) Parallel processing in retinal ganglion cells: How integration of space-time patterns of excitation and inhibition form the spiking output. *J Neurophysiol* 95:3810–3822.
8. Amthor FR, Takahashi ES, Oyster CW (1989) Morphologies of rabbit retinal ganglion cells with complex receptive fields. *J Comp Neurol* 280:97–121.
9. Cleland BG, Levick WR (1974) Properties of rarely encountered types of ganglion cells in the cat's retina and an overall classification. *J Physiol* 240:457–492.
10. Mastronarde DN (1985) Two types of cat retinal ganglion cells that are suppressed by contrast. *Vision Res* 25:1195–1196.
11. Rowe MH, Stone J (1976) Properties of ganglion cells in the visual streak of the cat's retina. *J Comp Neurol* 169:99–125.
12. Famiglietti EV (2009) Bistratified ganglion cells of rabbit retina: neural architecture for contrast-independent visual responses. *Vis Neurosci* 26:195–213.
13. Roska B, Werblin F (2001) Vertical interactions across ten parallel, stacked representations in the mammalian retina. *Nature* 410:583–587.
14. Rockhill RL, Daly FJ, MacNeil MA, Brown SP, Masland RH (2002) The diversity of ganglion cells in a mammalian retina. *J Neurosci* 22:3831–3843.
15. Eccles JC, Llinás R, Sasaki K (1966) The excitatory synaptic action of climbing fibres on the purinje cells of the cerebellum. *J Physiol* 182:268–296.
16. Schmolesky MT, Weber JT, De Zeeuw CI, Hansel C (2002) The making of a complex spike: Ionic composition and plasticity. *Ann N Y Acad Sci* 978:359–390.
17. Gilbert PF, Thach WT (1977) Purkinje cell activity during motor learning. *Brain Res* 128:309–328.
18. Deschênes M, Roy JP, Steriade M (1982) Thalamic bursting mechanism: An inward slow current revealed by membrane hyperpolarization. *Brain Res* 239:289–293.
19. Roberts MT, Bender KJ, Trussell LO (2008) Fidelity of complex spike-mediated synaptic transmission between inhibitory interneurons. *J Neurosci* 28:9440–9450.
20. Welsh JP, Llinás R (1997) Some organizing principles for the control of movement based on olivocerebellar physiology. *Prog Brain Res* 114:449–461.
21. Taylor WR, Vaney DI (2002) Diverse synaptic mechanisms generate direction selectivity in the rabbit retina. *J Neurosci* 22:7712–7720.
22. van Wyk M, Taylor WR, Vaney DI (2006) Local edge detectors: a substrate for fine spatial vision at low temporal frequencies in rabbit retina. *J Neurosci* 26:13250–13263.
23. Kanjhan R, Vaney DI (2008) Semi-loose seal Neurobiotin electroporation for combined structural and functional analysis of neurons. *Pflugers Arch* 457:561–568.
24. Borg-Graham LJ (2001) The computation of directional selectivity in the retina occurs presynaptic to the ganglion cell. *Nat Neurosci* 4:176–183.
25. Vaney DI (1990) The mosaic of amacrine cells in the mammalian retina. *Prog Ret Res* 9: 49–100.
26. Caldwell JH, Daw NW, Wyatt HJ (1978) Effects of picrotoxin and strychnine on rabbit retinal ganglion cells: Lateral interactions for cells with more complex receptive fields. *J Physiol* 276:277–298.
27. Thach WT (1968) Discharge of Purkinje and cerebellar nuclear neurons during rapidly alternating arm movements in the monkey. *J Neurophysiol* 31:785–797.
28. Swensen AM, Bean BP (2003) Ionic mechanisms of burst firing in dissociated Purkinje neurons. *J Neurosci* 23:9650–9663.
29. Kim Y, Trussell LO (2007) Ion channels generating complex spikes in cartwheel cells of the dorsal cochlear nucleus. *J Neurophysiol* 97:1705–1725.
30. Tazerart S, Vinay L, Brocard F (2008) The persistent sodium current generates pacemaker activities in the central pattern generator for locomotion and regulates the locomotor rhythm. *J Neurosci* 28:8577–8589.
31. Margolis DJ, Detwiler PB (2007) Different mechanisms generate maintained activity in ON and OFF retinal ganglion cells. *J Neurosci* 27:5994–6005.
32. Berson DM, Dunn FA, Takao M (2002) Phototransduction by retinal ganglion cells that set the circadian clock. *Science* 295:1070–1073.
33. Dacey DM, et al. (2005) Melanopsin-expressing ganglion cells in primate retina signal colour and irradiance and project to the LGN. *Nature* 433:749–754.
34. Khaliq ZM, Raman IM (2005) Axonal propagation of simple and complex spikes in cerebellar Purkinje neurons. *J Neurosci* 25:454–463.
35. Monsivais P, Clark BA, Roth A, Häusser M (2005) Determinants of action potential propagation in cerebellar Purkinje cell axons. *J Neurosci* 25:464–472.
36. Tzounopoulos T, Kim Y, Oertel D, Trussell LO (2004) Cell-specific, spike timing-dependent plasticities in the dorsal cochlear nucleus. *Nat Neurosci* 7:719–725.
37. Lisman JE (1997) Bursts as a unit of neural information: Making unreliable synapses reliable. *Trends Neurosci* 20:38–43.
38. Stone J, Fukuda Y (1974) Properties of cat retinal ganglion cells: A comparison of W-cells with X- and Y-cells. *J Neurophysiol* 37:722–748.
39. Dodt H, Eder M, Frick A, Zieglgänsberger W (1999) Precisely localized LTD in the neocortex revealed by infrared-guided laser stimulation. *Science* 286:110–113.
40. Rae J, Cooper K, Gates P, Watsky M (1991) Low access resistance perforated patch recordings using amphotericin B. *J Neurosci Methods* 37:15–26.